Ibn Al-Haitham Journal for Pure and Applied Sciences
Journal homepage: jih.uobaghdad.edu.iq
PISSN: 1609-4042, EISSN: 2521-3407
IHJPAS. 2025, 38(2)

Preparing Indium Films and Studying the Effect Oxidation on Their Properties

Mohmmad H. Faisal[1*] and Seham H. Salman[2]
[1,2]Department of Physics, College of Education for Pure Science (Ibn Al-Haitham), University of Baghdad, Baghdad, Iraq.
[*]Corresponding Author.

Received : 11 May 2024 Accepted: 10 September 2024 Published: 20 April 2025
doi.org/10.30526/38.2.4010

Abstract

This research dealt with the preparation and study of the properties of (In_2O_3) as a film. Indium films were used by the vacuum thermal evaporation technique on a glass base, and then these films were thermally treated at a temperature of 300 in the presence of oxygen for some time (30, 60, 90, 120) minutes to obtain films. Through X-ray diffraction examinations, atomic force microscopy, and ultraviolet radiation, the thin, transparent indium films revealed that the prepared films are cubic crystalline semiconducting materials. The dominant orientation of this crystal is 222, and the energy gap ranges between 2.1 and 2.7 eV. It can be prepared in the form of a film and varies with the oxidation times and depends on the surface roughness and the root mean square of the roughness. The grain size depends on the oxidation period with constant temperature and oxygen pumping rate, as is clear from the atomic force microscope images attached to the research.

Keywords: In, In_2O_3, Thin films, Thermal oxidation, Thermal evaporation.

1. Introduction

Indium oxide is considered a semiconductor material (1). It is a transparent oxide (TCO) (2) with an indirect Eg of 3.5 electron volts and an indirect Eg of 2.5 electron volts (3). By evaporating the indium material on glass or silicon bases in a vacuum chamber (4), one can prepare it as a yellow powder or film (5) from the air and then oxidize the membrane using one of the oxidation methods (6), including the rapid thermal oxidation method under normal weather conditions (7). Indium reacts with oxygen to form indium oxide (In_2O_3) in the following equation: $2In(s) + 3O = In_2O_3$ (8).The presence of additional indium atoms or oxygen holes in indium oxide makes it a donor (n-type donor) (9). The In2O3 film is used as an anti-reflective window layer on the surfaces of solar cells. It is a regular and transparent film (about 80% in the visible region (0.4-0.9 µm)). It has high reflectivity in the IR region and is, therefore, a heat-reflecting window (9-12). It is also a polycrystalline membrane with a cubic structure and has a lattice constant of 10.118 Å) according to the American standard (ASTM) (13).
Indium(III) oxide is insoluble in both water and alkalis (14), but it can dissolve in acids (15),

transparent reflectors of hot mirrors, as a transparent conductive paint in combination with tin dioxide (SnO_2) (16), and it is also used in integrated circuits (as a resistive element)(17).

2. Materials and Methods

Indium oxide In_2O_3 thin films were fabricated using the thermal oxidation process. The initial stage was the deposition of tiny layers of indium metal via vacuum thermal evaporation. The process of evaporation was conducted. in a state of low pressure of order of $2*10^{-5}$mbar. The deposit rate is approximately 1.33±0.2 nm/sec. , the distance (18 cm) between the Mo boat and the substrate. The indium thin films of thickness 400 nm (total surface area 2 × 2 mm). The second phase, which involved the thermal oxidation of a thin layer of In, was carried out. (30, 60, 90, and 120) min. at 300 °C in the presence of O2. By employing a flat electric heater to provide heat to the substrate. The films were analyzed for crystallinity and the presence of crystalline phases using X-ray diffraction (XRD) with a CuKα X-ray diffractometer. (Shimadzu Japan -XRD600). The measurement of the absorbance and transmittance of the formed thin film was conducted utilizing. The UV-visible 1800 spectra photometer measures wavelengths within a specific range. spans from 200 to 1100 nm. With a resolution of more than 300 dpi and less than 600 dpi and without borders, with the capital first letter of axis titles and write its unit. Tables and Figures are placed in the results in the sequence mentioned, not at the end of the manuscript.

3. Results and Discussion

3.1. The Analysis Using X-Ray Diffraction (XRD)

Figure 1 as seen in the X-ray diffraction. The rhombohedral structure of thin film polycrystalline material as in. Diffraction data relates to the [011]'s existence. Diffraction peaks are found in crystalline materials. The evaporation of the metallic material occurred at an angle of 32.9822° concerning 2θ. Following oxidation in **Figure 2**, the films (In_2O_3) exhibited a polycrystalline cubic structure. The videos have notable peaks at 21.448°, 30.515°, and 35.38° in the pacified order, matching the (112), (222), and (004) planes. These peaks match or are equal. to cubic. The JCPDS card 98-064-0179 identifies the chemical as indium oxide. The (222) line's preferred orientation. The result corresponds with that described by (18-20). From the x-ray, it is possible to see that the intensity increases with increasing oxidation time, indicating enhanced crystalline structure and crystalline size modification.

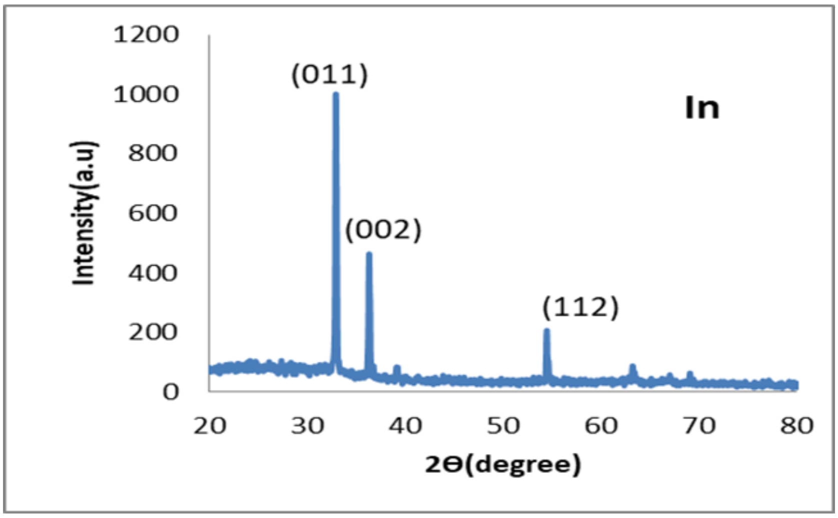

Figure 1. X-ray diffraction of the In film before oxidation.

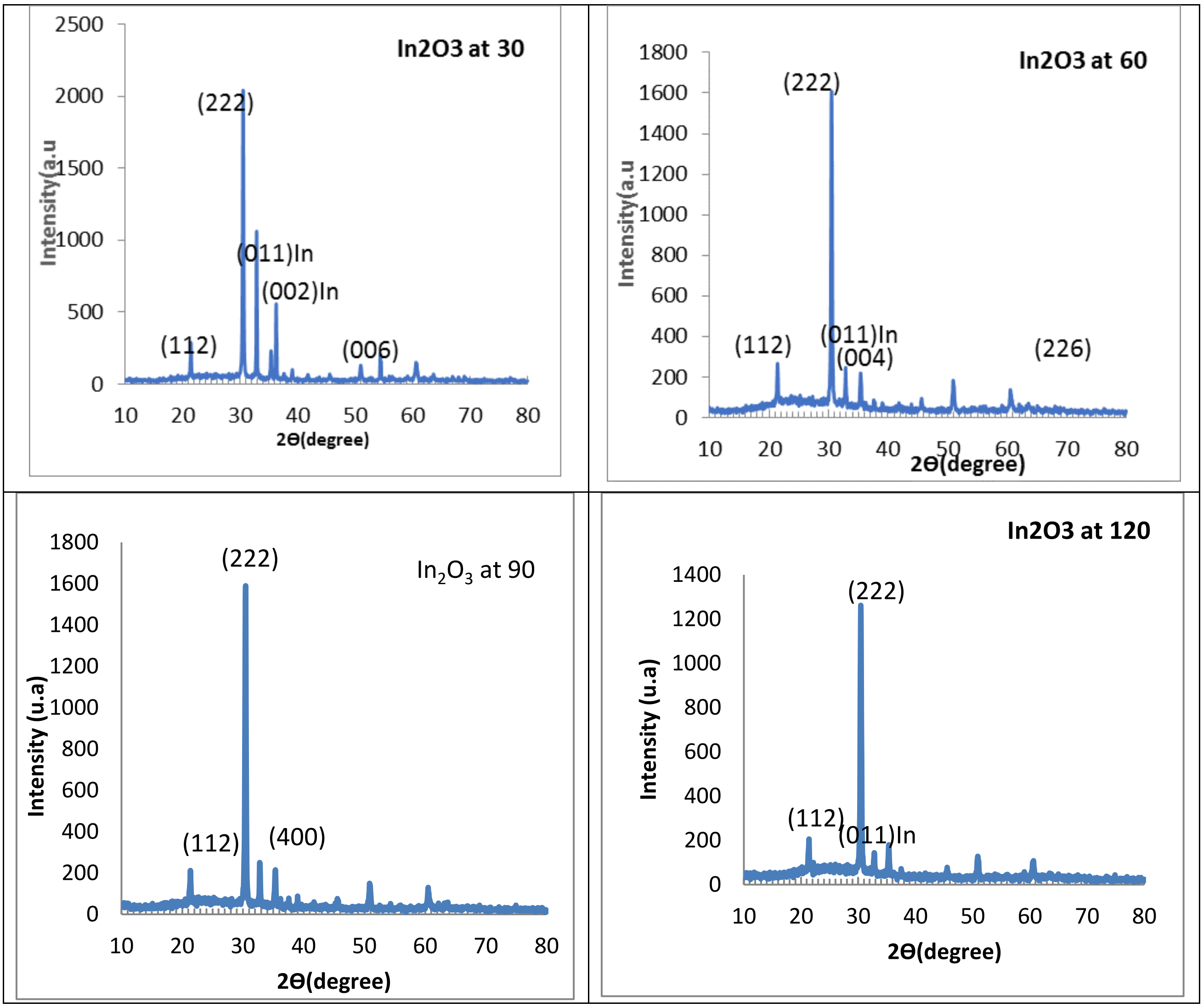

Figure 2. X-ray diffraction of the In2O3 film at different oxidation times.

Table 1. It is clear. X-ray diffraction traces for In2O3 thin film oxidation .

JCPDS card No.	Oxidation Time(min)	Temp.	2θ Exp.	2θ ASTM	d-Exp.	d ASTM	Hkl
98-064-0179	30	300	30.5672	30.515	2.92226	2.92717	222
	60		30.5596		2.92297		
	90		30.4452		2.9337		
	120		30.4745		2.93094		

The (222) line's orientation in the XRD peaks was To ascertain the structural properties, including variables like the crystalline C.s., the dislocation density, and the mean lattice strain ε Considering the dislocation density as well as the quantity of crystallites in each area, the following relationships need to be considered (21-27).The information is included in **Table 2**.

$$C.s = 0.9\lambda / (\beta Cos\theta) \quad (1)$$

$$\delta = 1/ (C.s)^{2} \quad (2)$$

$$\varepsilon = \beta\ Cos\theta / 4 \quad (3)$$

$$No = t/(C.s)^{3} \quad (4)$$

where the breadth at half its high intensity is represented by β. The thin layer's thickness is represented by the variable "t".

Table 2. lists the relevant characteristics, which include the number of crystallites, macrostrain, density of dislocations, and size of the crystallites. Which Oxidation at various moments.

Oxidation time (min).	**2Θ**	**β (deg)**	**β (rad)**	**C.s(nm)**	**δ (nm)$^{-2}$**	**ε**	**N_o (nm)$^{-2}$**
30	30.5672	0.1943	0.003389	44.27479	0.00051	0.000817	0.004609
60	30.5596	0.2125	0.003707	40.48206	0.00061	0.000894	0.006029
90	30.4452	0.1897	0.003309	45.33524	0.00048	0.000798	0.004293
120	30.4745	0.2483	0.004331	34.63832	0.00083	0.001045	0.009625

3.2. Surface Morphology

One of the most applicable methods for surface morphology is Atomic Force Microscopy (AFM). It is well known that the surface morphology of films affects their properties, which is crucial for applications like gas sensing. It shows the presence of homogenous grains throughout the film. are shown in **Table 3**. As a result, it is crucial to look into the surface morphology of films because increasing surface roughness of the films. The appearance of the surface of the In_2O_3

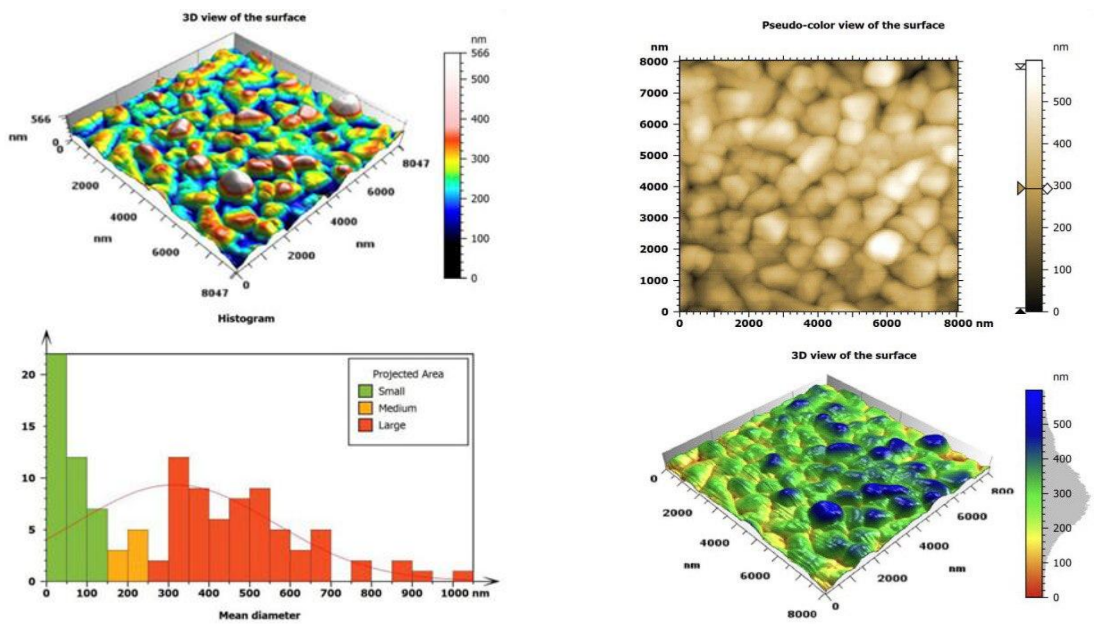

Figure 3. AFM for In2O3 at 30 min.

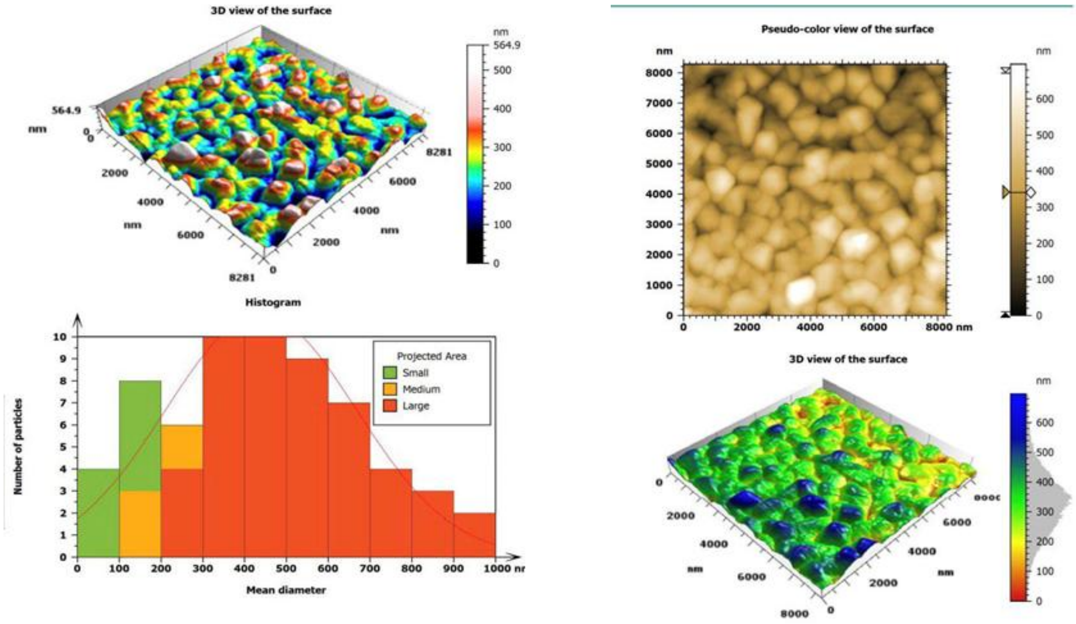

Figure 4. AFM for In2O3 at 60 min.

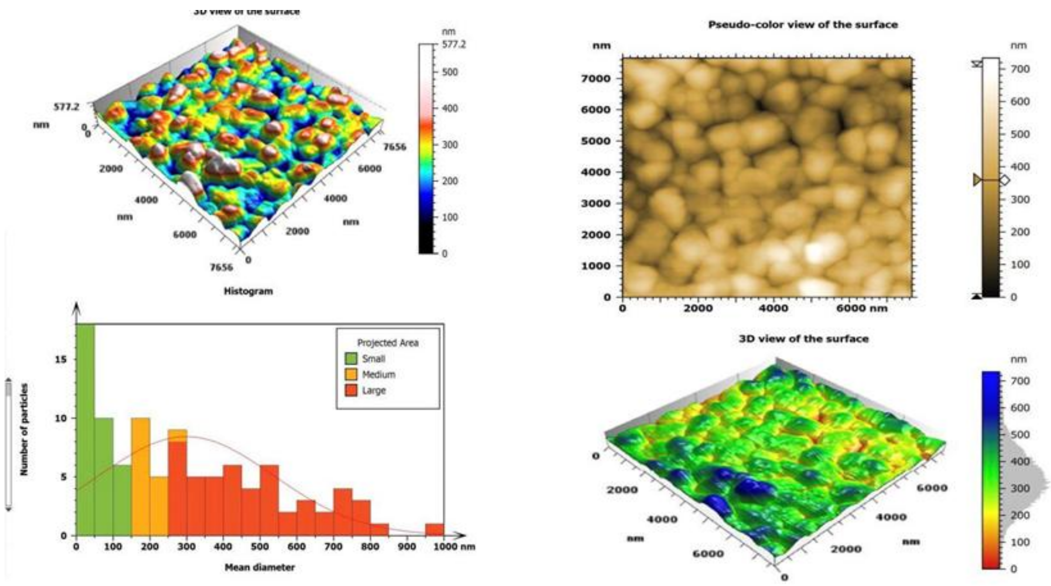

Figure 5. AFM for In2O3 at 90 min.

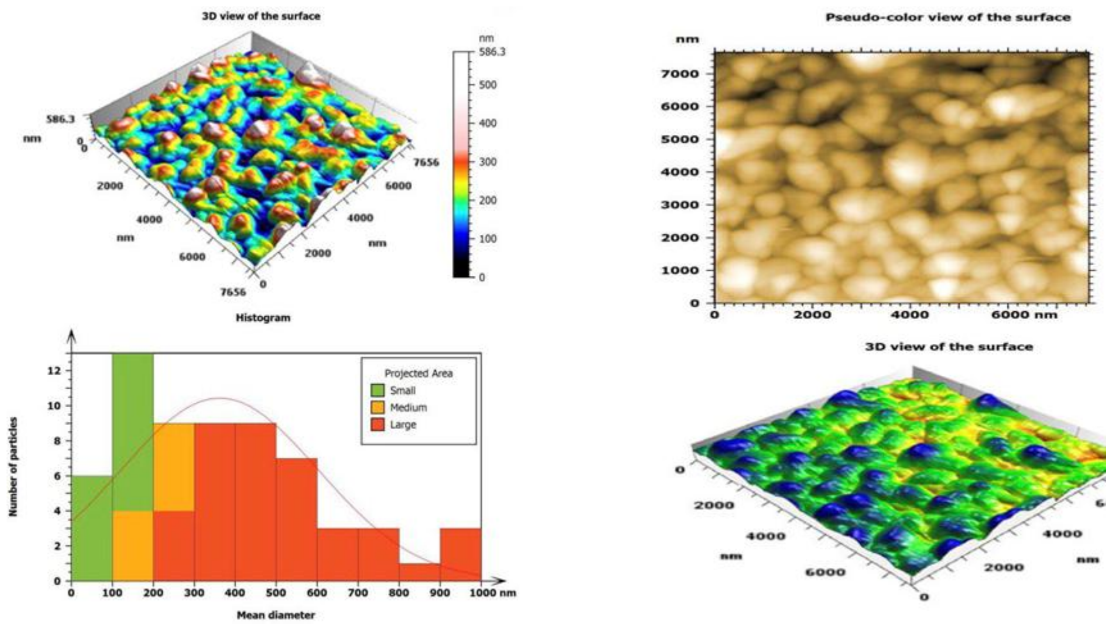

Figure 6. AFM for In2O3 at 120 min.

Table 3. Mean diameter, roughness and root mean square at different times.

oxidation times (min)	Mean diameter (nm)	Roughness(nm)	Root-mean-square (nm)
30	315.9	68.62	86.18
60	439.4	77.32	98.26
90	299.0	76.82	97.79
120	362.1	78.43	96.67

From the table above, we find that the surface roughness rate is better when the feeding duration is 30 minutes, as well as the square root of the roughness. As for the size of the particles or the diameter of the lung, we obtain a larger amount when the oxidation time is 60 minutes.

3. 3.Optical Characteristics

Figure 3 shows the transmittance and absorbance spectra, which were quantified to examine the optical properties. According to our research, the film shows excellent transmission at long wavelengths and poor transmission at short wavelengths. We notice from the figure that if the oxidation time is short, the transmission value is lower and increases as it increases.

This means that absorption reaches its peak at a low value of wavelength, that is, within the beginning of the visible light. It is possible to benefit from In_2O_3In thin films in the manufacture of solar cells and photodiodes due to their high absorption.

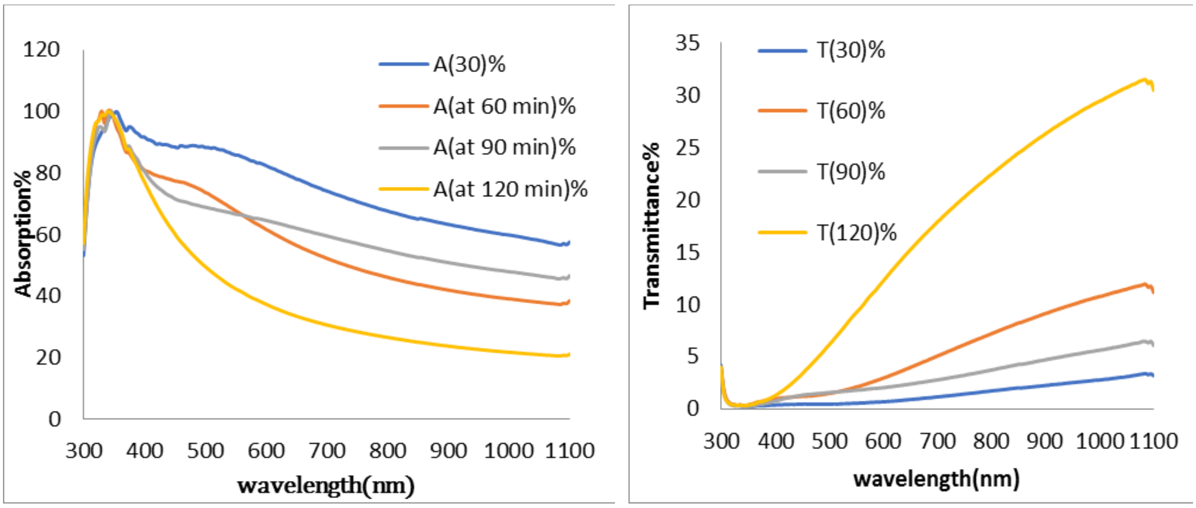

Figure 7. Absorption and transmittance of In2O3 at different oxidation times.

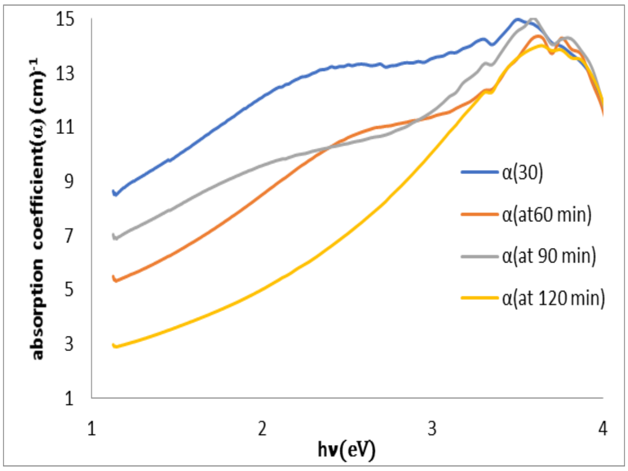

Figure 8. The variation (α) with h**ν** for In2O3 thin films.

Absorption coefficient determined by equation (5)(28):

$\alpha = 2.303A/t$ (5)

The equation(6) was used to find the extinction coefficient (K) of In_2O_3 (29)

$K = \alpha\lambda / 4\pi$ (6)

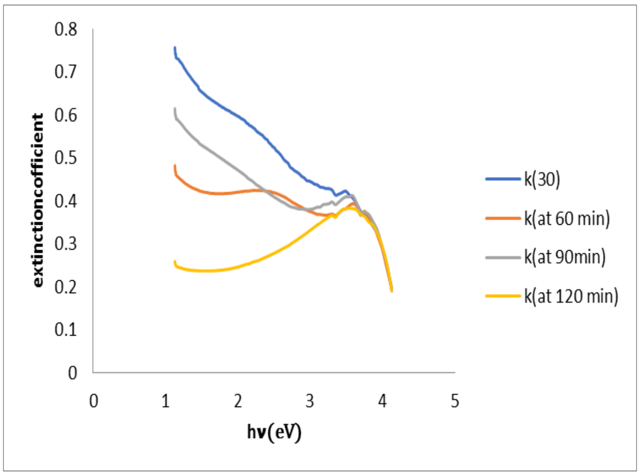

Figure 9. Illustrates the relationship between the extinction coefficient and Energy for In2O3 thin films.

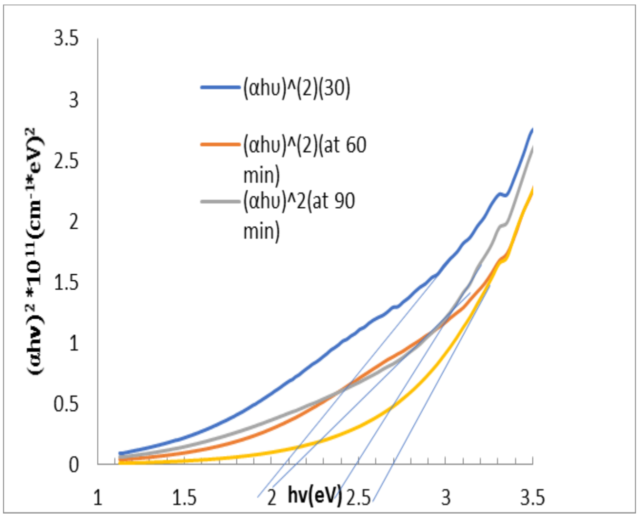

Figure 10. Plot of (αhυ) ^{2} versus (hυ) for In_2O_3 thin films.

The energy gap was computed via Tauck's.(29-32)

$(\alpha h\nu)=B(h\boldsymbol{\nu}-Eg)^{n}$ (7)

Here is how the equation is defined: The constant denoted by the symbol (B) and the exponent represented by the symbol (n) are established by the material's particular quantum selection criteria.Plot the relationship between hν and $(\alpha\ h\nu)^2$ to find the direct band gap. **Figure 6** illustrates this. **Table 3** shows that the optical band gap energy of the film was determined to be 2.1, 2.15, 2.5, and 2. 7 eV. The energy gap increases with increasing oxidation time; this is due to a greater width of the tails of the localized states, which may not be considered suitable for dangling bonds during the process of growth and crystal formation, as shown in the table below **Table 3.**

Table 4. Bandgap variation of In_2O_3 thin films with different oxidation times.

oxidation times (min)	Eg(eV)
30	2.1
60	2.15
90	2.5
120	2.7

4. Conclusion

Indium oxide thin films with different time oxidation have been successfully deposited after oxidation by the evaporation technique on glass substrates. The effect of oxidation time on properties was investigated. (In_2O_3) exhibited a polycrystalline cubic structure. These peaks match or are equal. The (222) line's preferred orientation. We find that the surface roughness rate is better when the feeding duration is 30 minutes. The optical band gap energy of the film was determined to be 2.1, 2.15, 2.5, and 2. 7 eV. The energy gap increases with increasing oxidation time.

Acknowledgment

We thank the Thin Film Lab., Department of Physics, College of Education for Pure Science (Ibn Al-Haitham), University of Baghdad.

Conflict of Interest

The authors declare that they have no conflicts of interest.

Funding

None.

References

1. Kim J, Shrestha S, Souri M, Connell JG, Park S, Seo A. High-temperature optical properties of indium tin oxide thin-films. Sci Rep. 2020;10(1):12486. https://www.nature.com/articles/s41598-020-69463-4.
2. Al-Kuhaili MF. Electrical conductivity enhancement of indium tin oxide (ITO) thin films reactively sputtered in a hydrogen plasma. J Mater Sci Mater Electron. 2020;31(4):2729-2740. https://doi.org/10.1007/s10854-019-02813-9.
3. Jassim AS, Rashid SN, Yaseen HM. Effect of CO2 laser irradiation on the topographic and optical properties of CdO thin films. Baghdad Sci J. 2020;17(1):318-328. https://doi.org/10.21123/BSJ.2020.17.1(SUPPL.).0318.
4. Dahham AT, Aadim KA, Abbas NK. Synthesis and fabrication of In2O3:CdO nanoparticles for NO2 gas sensor. Baghdad Sci J. 2018;15(3):292-299. https://doi.org/10.21123/bsj.2018.15.3.0292.
5. Choopun S, Hongsith N, Wongrat E. Metal-oxide nanowires for gas sensors. Nanowires-Recent Advances. 2012:3-24. http://dx.doi.org/10.5772/54385.
6. Jhong HRM, Nwabara UO, Shubert-Zuleta S, Grundish NS, Tandon B, Reimnitz LC, Milliron DJ. Efficient aqueous electroreduction of CO2 to formate at low overpotential on indium tin oxide nanocrystals. Chem Mater. 2021;33(19):7675-7685. https://doi.org/10.1021/acs.chemmater.1c01649.
7. Mohamed WS, Ali HM, Adam AG, Shokr EK. Vacuum-evaporated PbS:0.03 Zn thin films with varying thicknesses for environmental applications. Opt Mater (Amst). 2024;148:114885. https://doi.org/10.1016/j.optmat.2024.114885.
8. Horoz B, Tuna Yıldırım S, Soltabayev B, Ateş A, Acar S, Yıldırım MA. Effect of SILAR cycle on gas sensing properties of In2O3 thin films for CO gas sensor. J Mater Sci Mater Electron. 2024;35(2):163. https://doi.org/10.1007/s10854-024-11970-5.
9. Vaishnav VS, Patel SG, Panchal JN. Development of indium tin oxide thin film toluene sensor. Sens Actuators B Chem. 2015;210:165-172. https://doi.org/10.1016/j.snb.2014.11.075.
10. Adurodija FO, Izumi H, Ishihara T, Yoshioka H, Matsui H, Motoyama M. High-quality indium oxide films at low substrate temperature. Appl Phys Lett. 1999;74(20):3059-3061. https://doi.org/10.1063/1.124064.
11. Kiriakidis G, Katsarakis N, Bender M, Gagaoudakis E, Cimalla V. InOx thin films, candidates for novel chemical and optoelectronic applications. Mater Phys Mech. 2000;1:83-98. https://doi.org/10.1021/acs.chemmater.1c01649.
12. Kamimori T, Nagai J, Mizuhashi M. Electrochromic devices for transmissive and reflective light control. Sol Energy Mater. 1987;16(1-3):27-38. https://doi.org/10.1016/0165-1633(87)90005-0.
13. Oleiwi HF, Rahma AJ, Salih SI, Beddai AA. Comparative study of sol-gel and green synthesis technique using orange peel extract to prepare TiO2 nanoparticles. Baghdad Sci J. 2024;21:1702. https://doi.org/10.21123/bsj.2023.8089.
14. Adurodija FO, Izumi H, Ishihara T, Yoshioka H, Matsui H, Motoyama M. High-quality indium oxide films at low substrate temperature. Appl Phys Lett. 1999;74(20):3059-3061. https://doi.org/10.1063/1.124064.
15. Makadsi MN. Recent progress in doped a-Si prepared by thermal evaporation. In: Energy and the Environment. Elsevier; 1990. p. 164-169. https://doi.org/10.1016/B978-0-08-037539-

7.50023-5.
16. Marezio M. Refinement of the crystal structure of In2O3 at two wavelengths. Acta Crystallogr. 1966;153:324. https://doi.org/10.1107/S0365110X66001749.
17. Clark AH, Kazmerski LL. Polycrystalline and amorphous thin films and devices. 1980. https://books.google.com/books?hl=ar&lr=&id=40tj3r8rEmcC&oi=fnd&pg=PP1&dq=Clark,+A.H.%3B+Kazmerski,+L.L.+Polycrystalline+and+Amorphous+Thin+Films+and+Devices+1980.
18. Sze SM, Lee MK. 3rd ed. Semiconductor Devices: Physics and Technology. 3rd ed. Wiley; 2002.
19. Alizadeh A, Rajabi Y, Bagheri–Mohagheghi MM. Effect of crystallinity on the nonlinear optical properties of indium–tin oxide thin films. Opt Mater (Amst). 2022;131:112589. https://doi.org/10.1016/j.optmat.2022.112589.
20. Mattes BL, Kazmarsk L. Polycrystalline and amorphous thin films and devices. 1980.
21. Abbas ZM, Abbas QA. Influence of a magnetic field on the structure, morphology, and gas sensing characteristics of ZnO:Al thin films prepared by pulsed laser ablation. Iraqi J Sci. 2024;65:2007-2019. https://doi.org/10.24996/ijs.2024.65.4.19.
22. Hadi AJ, Nayef UM, Jabir MS, Mutlak FA-H. Laser-ablated tin dioxide nanoparticle synthesis for enhanced biomedical applications. Plasmonics. 2023;18(5):1667-1677. https://doi.org/10.1007/s11468-023-01888-9.
23. Salman SH, Ali SM, Ahmed GS. Study the effect of annealing on structural and optical properties of indium selenide (InSe) thin films prepared by vacuum thermal evaporation technique. J Phys Conf Ser. 2021;1879(3):032058. https://doi.org/10.1088/1742-6596/1879/3/032058.
24. Salman SH, Hassan NA, Ahmed GS. Copper telluride thin films for gas sensing applications. Chalcogenide Lett. 2022;19(2):125-130. https://doi.org/10.15251/cl.2022.192.125.
25. Ali IM, Al-Jenabi MA. Structural and optical properties of In2O3 and indium tin oxide thin films. J Univ Anbar Pure Sci. 2017;11(1). https://www.iasj.net/iasj/download/7b01ac131b6e8710.
26. Callister Jr WD, Rethwisch DG. Fundamentals of Materials Science and Engineering: An Integrated Approach. John Wiley & Sons; 2020. https://books.google.com/books?hl=ar&lr=&id=rh7zDwAAQBAJ&oi=fnd&pg=PR21&dq=Callister+Jr,+W.D.%3B+Rethwisch,+D.G.+Fundamentals+of+Materials+Science+and+Engineering:+An+Integrated+Approach%3B+John+Wiley+%26+Sons,+2020%3B+ISBN+1119723671.
27. Omer MA. Elementary Solid State Physics. John Wiley 1990, 233, 112-123.
28. Sari WP, Agbroko SO, Covington JA. Semiconducting indium oxide sensor for oxygen detection. In: Proceedings of the 2021 IEEE Region 10 Symposium (TENSYMP); IEEE; 2021. p. 1-4. https://doi.org/10.1109/TENSYMP52854.2021.9550813.
29. Mohammed NJ, Rasheed ZS. Enhancement optical characterization of tin oxide in polymer polyvinyl alcohol colloid prepared by laser ablation method. Baghdad Sci J. 2024; *21*:2425-2432.https://doi.org/10.21123/bsj.2023.8494.
30. Callister Jr WD, Rethwisch DG. Fundamentals of Materials Science and Engineering: An Integrated Approach. John Wiley & Sons; 2020. ISBN 1119723671.
31. Salman SH, Alhuda N, Ghuzlan H, Ahmed S, Mohammed HI, Abbas SA. Effect of annealing time on physical properties of TiO2 thin films prepared by RF magnetron sputtering technique. 2024;20(1):37-42.
32. Sundaresh S, Nehate SD, Sundaram KB. Electrical and optical studies of reactively sputtered indium oxide thin films. ECS J Solid State Sci Technol. 2021;10(6):065016. https://doi.org/10.1149/2162-8777/ac0a51.